Materials Physics and Mechanics 42 (2019) 211-223 Received: March 3, 2018

THE STRUCTURAL TRANSFORMATION AND MECHANICAL STRENGTH OF Ni, Ti NANOWIRES AND NITINOL ALLOYS AT VARIOUS VACANCY RATES: MOLECULAR DYNAMIC STUDY USING CLERI-ROSATO POTENTIAL

M.M. Aish*

Physics department, Faculty of science, Menoufia university, Egypt

*e-mail: mohamedeash2@yahoo.com

Abstract. A many-body interatomic potential was used for Nickel (Ni) crystal with face-centered cubic (FCC) lattice and Titanium (Ti) with hexagonal close-packed (HCP) lattice and Nitinol alloys within the second-moment approximation. The tight-binding model (the Cleri and Rosato potentials) was employed to carry out three dimensional molecular dynamics simulations upon application of uniaxial tension at nanoscale of studied materials, which contained various vacancy rates. We performed molecular dynamics (MD) simulations to study the yield mechanisms in Ni and Ti nanowires and Nitinol alloys. The coupled effects of various shapes, sizes, and locations of vacancy defects on the mechanical strength and structural deformation of nanowires are presented. The formation energies of vacancy defects are also evaluated. It was found that as the number of vacancies increases, the yield stress decreases. The results showed that breaking time changes with the increase in number of vacancy. To understand the effects of the vacancies on the mechanical properties of Ni and Ti nanowires and Nitinol alloys, tensile and fatigue tests are simulated.
Keywords: many-body, Nitinol, alloys, vacancy, defects

1. Introduction

MD simulations are used to simulate the movement of interacting atoms under the Newtonian mechanics. Given the instantaneous position and velocity vectors of the atoms, the dynamical history of the composition is generated by integrating the equations of motion numerically. The energy and force of the system are calculated. Computer simulation process was produced for systems under equilibrium, minimal interatomic energy and force through development of suitable interatomic potentials.

Vacancies which had little effect on the mechanical properties while seriously affecting the electrical properties. Vacancies Would be very effective in increasing the electrical resistance. Perhaps the clearest example of a phenomenon in which vacancies are created and absorbed by stationary edge dislocations is the Kirkendall effect. This explanation, however, requires that sources of vacancies should be presented within the grains of the alloy. The sources can only be dislocations (or grain boundaries), unless the vacancies condense in the form of macroscopic holes. The presence of such holes has in fact been reported in certain cases. The vacancies formed when dislocations move will bring slipping in the plane of a given Frank-Read source, even if no deformation bands are formed. It is shown that one has to expect cross-slip and formation of deformation bands.

http://dx.doi.org/10.18720/MPM.4222019_8

It is shown moreover that the formation of vacancies by moving dislocations plays an essential role in these processes. It is suggested that the movement of vacancies (self-diffusion) plays an essential role in polygonization, recovery and steady-state creep, enabling dislocations in deformation bands to move out of their slip planes and so relieve stress. Except by slipping right out of the crystal, it can disappear only by vacancy diffusion, which can remove the extra layer of atoms.

The mechanical properties of nanowires have been studied by use of nano indentation [1]. On the other hand, the mechanical properties of silicon carbide-silica biaxial nanowires and their structural transformation between a biaxial and coaxial configuration have been studied by use of transmission electron microscopy [2]. The mechanical properties of Ni nanowires dependence on size, shape, as well as the temperature have been studied [3-9]. Characterization of strain-induced structural transformations in CdSe nanowires using molecular dynamics simulation were also studied in [10].

This work was performed using our new MD program "Structural Transformation of Metallic FCC, BCC and HCP Nanowires and Their Alloys Using Cleri- Rosato potential". Ni and Ti nanowires and Nitinol alloys were taken as an object of investigation. The structures were presented in the form of a FCC for Ni, HCP for Ti and austenite for Nitinol alloys. The molecular dynamics method based on Cleri Rosato potential function [11,12] was used for calculation of the dynamics of the atomic structure in this paper.

2. Molecular dynamic potential: Cleri and Rosato

The interatomic interactions were calculated using the tight-binding potentials [11], we used a computer program for simulating a system involving several thousands of atoms in the time interval up to several nanoseconds. It should be noted that, even in the current state in the development of high-performance computers, an ab initio simulation of this system remains impossible. On the other hand, the potentials proposed by Cleri and Rosato [11] have already worked well in cluster studies [13–15]. In the EAM formalism, the binding energy of an i^{th} atom in a crystal with N atoms is a sum of contributions from the pair potential and embedding potential functions.

In our model, the potential energy of the system was calculated according to the relation:

$$U = \sum_i (E_b^i + E_r^i), \tag{1}$$

where

$$E_r^i = \sum_{j \neq i} U_{ij}(r_{ij}) = \sum_j A.\exp[-p(\frac{r_{ij}}{r_0} - 1)] \tag{2}$$

is the two-body term, and

$$E_b^i = -\sqrt{\sum_{j \neq i} \phi(r_{ij})}, \tag{3}$$

$$\phi(r_{ij}) = \zeta^2.\exp[2q(\frac{r_{ij}}{r_0} - 1)] \tag{4}$$

is the many-body term. In Eqs. (2)-(4), r_0 is the equilibrium distance between atoms, r_{ij} is the separation between the i^{th} and j^{th} atoms, and A, ξ, p, q are adjustable parameters governing the interaction between those atoms. These parameters (table 1 and 2) were taken directly from [11]. Eqs. (1) and (2) are similar to the Finnis-Sinclair (FS) scheme [13], but Eq. (1) uses a double summation convention for the repulsive functions, whereas the convention in the FS scheme is to sum this term for $j > i$ rather than $j \leq i$. For s, p-bonded metals there are no strong

theoretical motivation for representing the band energy part of the potential by a square-root term. However, this functional form can be rationalized as an empirical representation of the volume-dependent term required by the electron gas model of simple metals [11]. The length scale parameter r_0 in Eq. (1) is set to the lattice nearest neighbor distance. The remaining parameters (A, ξ, p, q) of the TB potentials were fitted for each element using the lattice constant, cohesive energy (E_J, elastic constants (C_{I1}, C_{I2}, C,) and vacancy formation energy (E").

Table 1. Parameters of tight-binding potentials for FCC metals. The potentials are cut off beyond the second neighbor distance ($r > \sqrt{2}r_0$)

	A (eV)	ξ (eV)	P	q	r_o	G/ ξ
Ni	0.0565	1.4005	14.0867	1.7937	2.4918	3.655

Table 2. Parameters of TB potentials for HCP Ti metals, parameters obtained with the experimental value, and theoretical fitting [12]

	A (eV)	ξ (eV)	P	q	r_o	G/ ξ
Ti (Ex)	0.1519	1.8112	8.620	2.390	2.896	3.936
Ti (Th)	0.0741	1.4163	11.418	1.643	2.896	3.936

The model can be used to describe quite well elastic, plastic, fracture and mechanical properties of a wide range of FCC, BCC and HCP-metals. The velocities of atomic motion in the simulation were determined using the Verlet algorithm. The potentials proposed by Cleri and Rosato [11] have already worked well in nanowires studies.

For a many-body attractive potential of the pair functional type (TB, EAM etc.), this normally entails joining one of the nodes of the function to an effective pair potential, V_{ij}, which was derived from a series expansion of the many-body potential in the bulk environment [16,22]. For TB potentials of the form of Eqs. (1)-(4), the effective pair potential acting between atoms i and j is given by:

$$V_{ij}(r_{ij}) = 2U_{ij}(r_{ij}) - \frac{\varphi(r_{ij})}{G} + \frac{[\varphi(r_{ij})]^2}{4G^3}. \quad (5)$$

Equation (5) assumes the usual pair potential evaluation convention. That interaction terms are only counted once for each distinct pair of atoms (in contrast to Eq. (1)). The functions $U_{ij}(r_{ij})$ and $\varphi(r_{ij})$ are defined in Eqs. (2) and (4) respectively. G is a lattice sum which represents the value of the total band energy associated with any atom k in the reference environment (normally a site in the bulk of the ideal lattice):

$$G = \sqrt{\sum_{k \neq l} \varphi(r_{kl})}. \quad (6)$$

The ratio G/ξ is dimensionless, for a lattice sum (Eq. (6)) corresponding to a bulk metallic environment. In all cases, this ratio takes values between 3.4 and 4.0. The larger values imply relatively greater long-range contributions to the potential. The attractive part of an effective pair potential derived for a surface environment may differ somewhat from that of a bulk environment, because of fewer contributions to the lattice sum in Eq. (6) [22]. However, this should have minimal impact on a composite potential designed for these

simulations, since the simulation was carried out at a separation where the repulsive part of the potential dominates.

In practical applications of TB potentials, it is also desirable to employ a switching function in order to terminate the potential and forces smoothly at the cut off distance, thereby preventing energy book-keeping errors due to the non-conservative nature of the many-body potential at the cut off distance. For this purpose, a simple polynomial switching function, *S(x),* can be applied to the potential in a region just below the cut off distance (rcut) [16]:

$$s(x) = 1 - 6x^5 + 15x^4 - 10x^3, \rightarrow r_{sw} \le r \le r_{cut}, \tag{7}$$

where $x = (r - r_{sw})/(r_{cut} - r_{sw})$, and r_{sw} is the distance at which the switching function was applied.

Finally, the TB potential formalism can be extended to describe bimetallic systems, using the fitting methods described in Refs. [12,16-19].

In general, the fitting parameters for a bimetallic system cannot be deduced from those of the pure elements alone. However, an approximate combination rule which has been used for TB and Finnis-Sinclair potentials may be useful in the absence of specific parameterizations [16,21]. This help for choosing the potential parameters in such way that the hetero-nuclear interaction terms (α-β, for elements α and β) correspond to the geometric means of the respective elemental terms (α- α, β- β):

$$\varphi^{\alpha\beta}(r_{ij}) = [\varphi^{\alpha\alpha}(r_{ij})\varphi^{\beta\beta}(r_{ij})]^{1/2}, \ldots U^{\alpha\beta} = [U^{\alpha\alpha}(r_{ij})U^{\beta\beta}(r_{ij})]^{1/2}. \tag{8}$$

The accuracy of this approximation needs to be evaluated on a case- by-case basis using suitable thermodynamic measures, and corrections may be required. This is an environment in which many-body potentials, despite their defect, are known to perform better than pair potentials [20]. When considering a closed system, the force acting on the i^{th} atom, will be:

$$F_i = -\sum_{i=1, i\neq j}^{N} \sum_{j=1}^{N} \frac{d\phi_{KL}(|r_i - r_j|)}{d(r_i - r_j)}. \tag{9}$$

Temperature of the atoms in a perfect crystal was calculated according to the relation:

$$T = \frac{2k}{3Nk_b} = \frac{1}{3Nk_b} \sum_{I}^{N} m_i v_i^2, \tag{10}$$

where k_b is the Boltzmann constant and k is the total Kinetic energy.

Computer simulation using a many-body interatomic potential for Ni and Ti nanowires and Nitinol alloys within the second-moment approximation of the tight-binding model (the Cleri and Rosato potentials) was employed to carry out three dimensional molecular dynamics simulations of the mechanical properties of Ni and Ti nanowires and Nitinol alloys. We studied the extension properties of investigated nanowires for different number of vacancies at 300K and 1000K, which was adjusted every 10^{-13} seconds. The estimated size of the crystal unit was for various experiments of 10 x 10 x 10, 12 x 12 x 12 and 18 x 18 x 18 atomic plane (AP). The average result is from 300 samples at 300 K and 1000 K.

It was assumed that the specimens have some random vacancies within materials in the simulation. The random distribution of vacancies were modeled by: (i) first calculating the number of vacancies according to the given vacancy fraction and the total atomic numbers; (ii) numbering the random vacancies in order; (iii) obtaining the occupation positions of the vacancies; (iv) converting the atoms and the vacancies to their actual positions in simulation. To understand the effects of the vacancies on the mechanical properties of Ni, Ti nanowires and Nitinol alloys, the tensile tests are simulated.

3. Results and discussion:

In this paper, the mechanical properties of nanoscale wires and their alloys were studied. Since the breaking and the yielding of Ni and Ti nanowires and Nitinol are of main interest in this work (Table 3), it seems to be reasonable to adopt small *Lx*, *Ly* and *Lz* for the simulations. To save the computing time, the dimensions of the MD models used in the following simulations are set to be *Lx=Ly=Lz*. The nature of deformation, slipping, twinning and necking were studied.

Three stages deformation. The experiments were obtained plots of the stored energy of deformation with the time, reflecting the processes in the nanowires during deformation. There are three stages of deformation: the quasi-elastic deformation (I), plastic deformation (II) until breaking, and failure (III). At all computer experiments, in the first stage there was almost linear increase in stress. The initial stage quasi-elastic area there is only relative displacement of atoms and there are no defects. Therefore, in this region the energy stored varies periodically.

FCC Ni nanowires at 300 K. First stage was completed at 16 ps for 10 x 10 x 10 Ni nanowires without vacancies, 11 ps, 10 Ps and 8 Ps, for vacancy rates equal 1%, 2% and 5%, respectively. The sharp fall takes place only at the point of transition from the first to second stages of deformation (Fig. 1 to 4). Experiments have shown that when the vacancy number increases the first stage of deformation was narrowed, and the second stage was also narrowed (Fig.1 to 4).

Table 3. The typical MD results of uniaxial tensile loading using Cleri-Rosato to 10 x 10 x 10 AP of Ni, Ti nanowires and Nitinol alloys at various vacancies at 300K, including the Yielding stress and breaking time

	vacancies V (%)	Yielding Stress σ (GPa)				Breaking time (t_b, Ps)			
		Ni	Ti		Nitinol	Ni	Ti		Nitinol
			Th	Ex			Th	Ex	
1	0.0	24	25	18	21	120	110	140	220
2	0.55	23	24.3	16.8	19	95	90	130	210
3	1	20	22	15	17	93	85	126	199
4	1.66	17	19.1	13.6	15	75	71	120	180
5	2	14	16	12	13	72	69	110	150
6	4	9	13	9	8	40	41	70	120
7	5	8	12	7	7	30	30	60	110
8	10	6	7	3	4	28	25	55	90

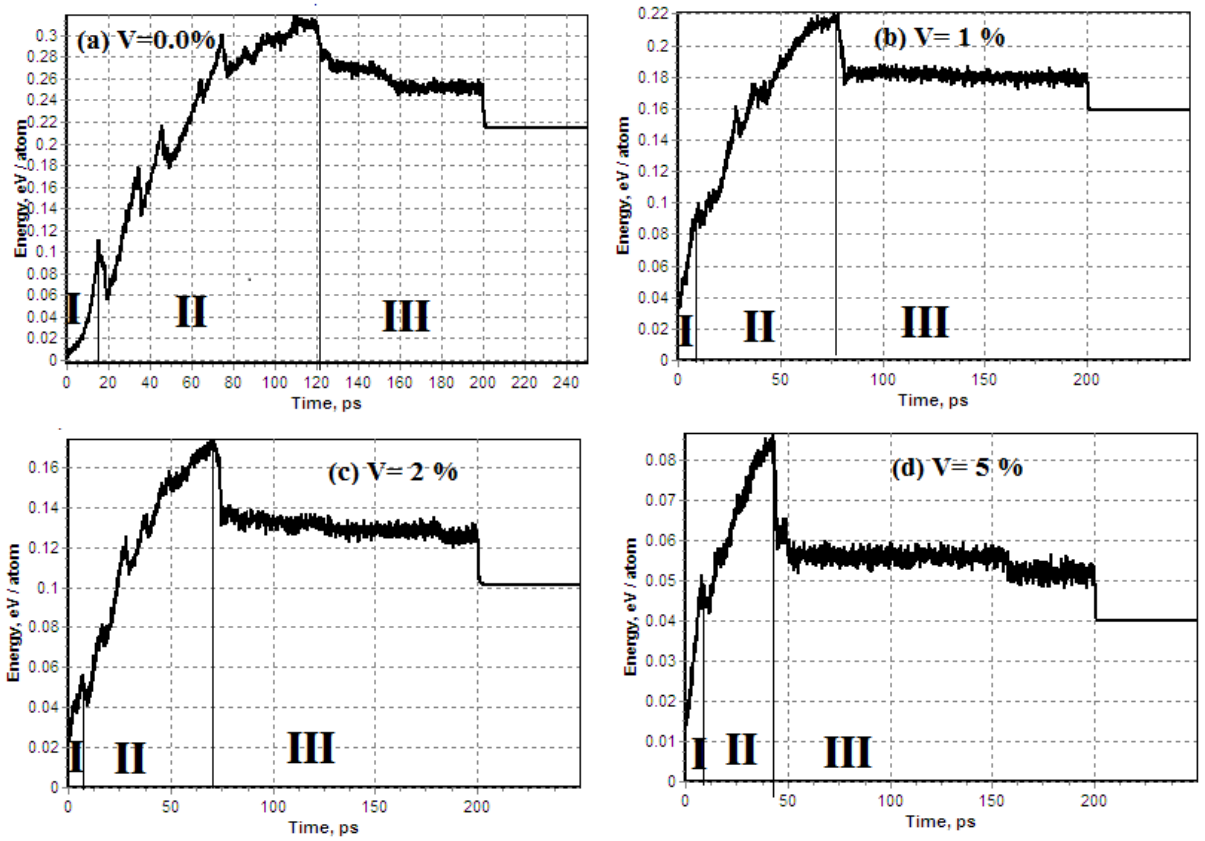

Fig. 1. The dependence of the stored energy of deformation at 300 K for FCC Ni 10 x 10 x 10 AP using Cleri-Rosato potential, a) without vacancies, b) V = 1%, c) V = 2% and d) V = 5%

Feature 12 x 12 x 12 AP of HCP Ti nanowires at 300K and 1000K. Figures 2, 3 indicates the change in the stored energy of the deformed crystal as a function of time at 300 K and 1000 K for 12 x 12 x 12 AP of HCP Ti nanowires at different vacancy concentrations. Experiments have shown that when the number of vacancies increases, the first stage of deformation narrowed, and the second stage also narrowed (Figs. 2 and 3).

Analysis of the graphs in Fig. 2 showed that the stored energy values at the peak of the strain curve at the end of the first stage for 0.0%, 1%, 2% and 5% vacancies rate of Ti nanowires are 0.09, 0.061, 0.05 and 0.046 eV / atom at 300 K, respectively. The level of stored energy at the end of the second stage (plastic deformation) for the investigated nanowire are 0.18, 0.109, 0.095 and 0.094 eV / atom at 300 K, respectively.

Analysis of the graphs in Fig. 3 showed that the stored energy values at the peak of the strain curve at the end of the first stage for 0.0%, 2%, 5% and 10% vacancies rate of HCP Ti 12 x 12 x 12 AP using theoretical value of Cleri-Rosato potential are 0.135, 0.132, 0.12 and 0.115 eV / atom at 1000 K, respectively. The level of stored energy at the end of the second stage (plastic deformation) for the investigated nanowire are 0.177, 0.164, 0.162 and 0.148 eV / atom at 1000 K, respectively.

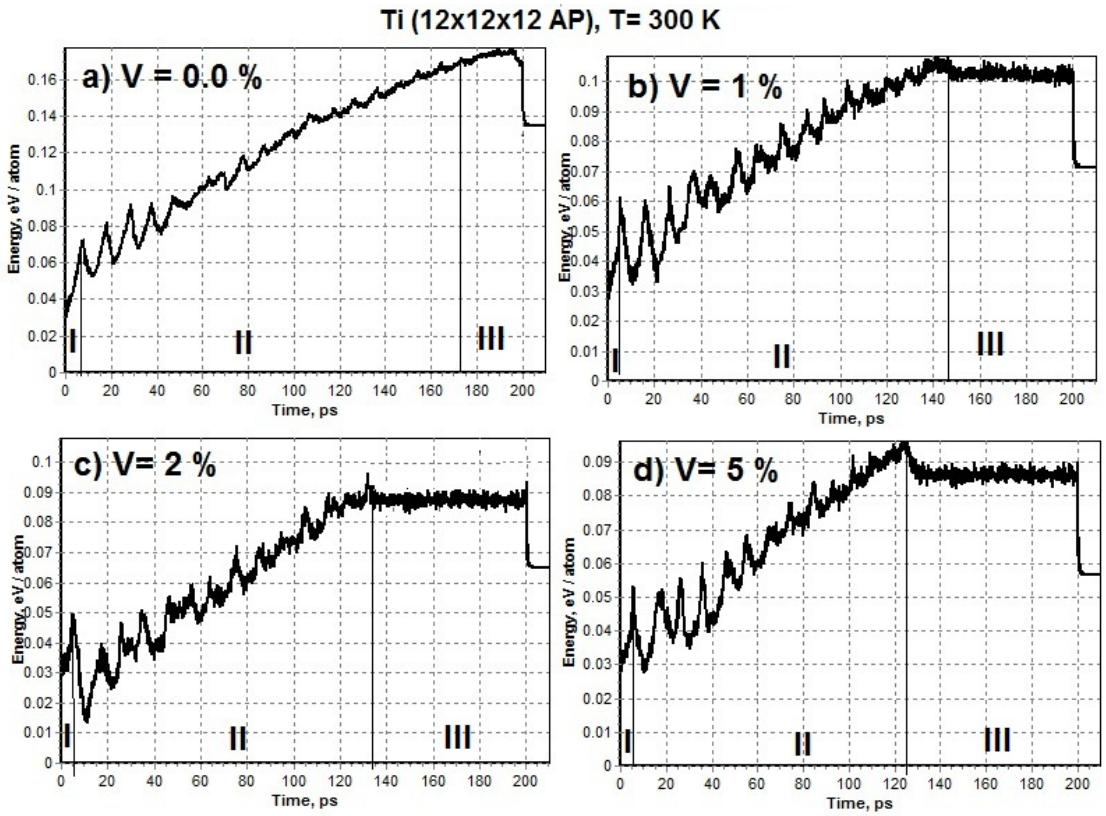

Fig. 2. The dependence of the stored energy of deformation at 300 K for HCP Ti 12 x 12 x 12 AP using theoretical value of Cleri-Rosato potential [11], a) without vacancies, b) V = 1%, c) V = 2% and d) V = 5%

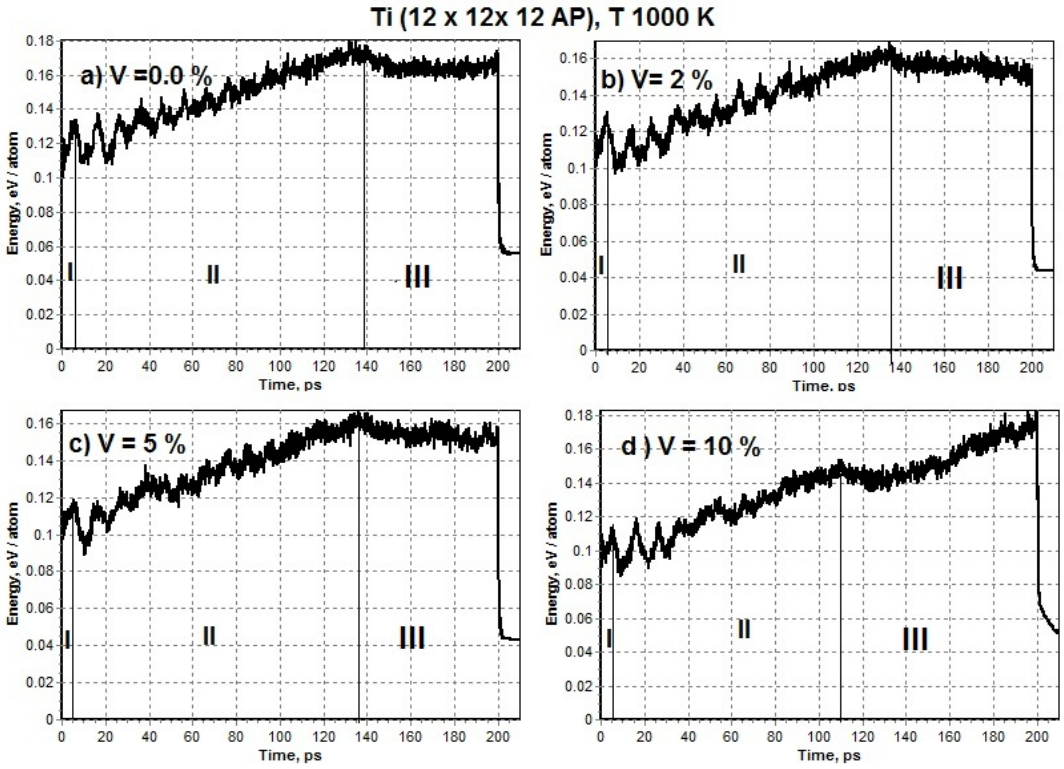

Fig. 3. The dependence of the stored energy of deformation at 1000 K for HCP Ti 12 x 12 x 12 AP using Experimental value of Cleri-Rosato potential [11], a) without vacancies, b) V = 2%, c) V = 5% and d) V = 10%

Feature of 18 x 18 x 18 AP of Nitinol alloys. Analysis of the graphs in Fig. 4 showed that the stored energy values at the peak of the strain curve at the end of the first stage at 0.0%, 1%, 5% and 10% vacancies rate of Nitinol alloy with size 18 x 18 x 18 AP are 0.06, 0.055, 0.043 and 0.04 eV / atom at 1000 K, respectively. The level of stored energy at the end of the second stage (plastic deformation) for the investigated nanwire are 0.12, 0.116, 0.11 and 0.111 eV / atom at 1000 K, respectively.

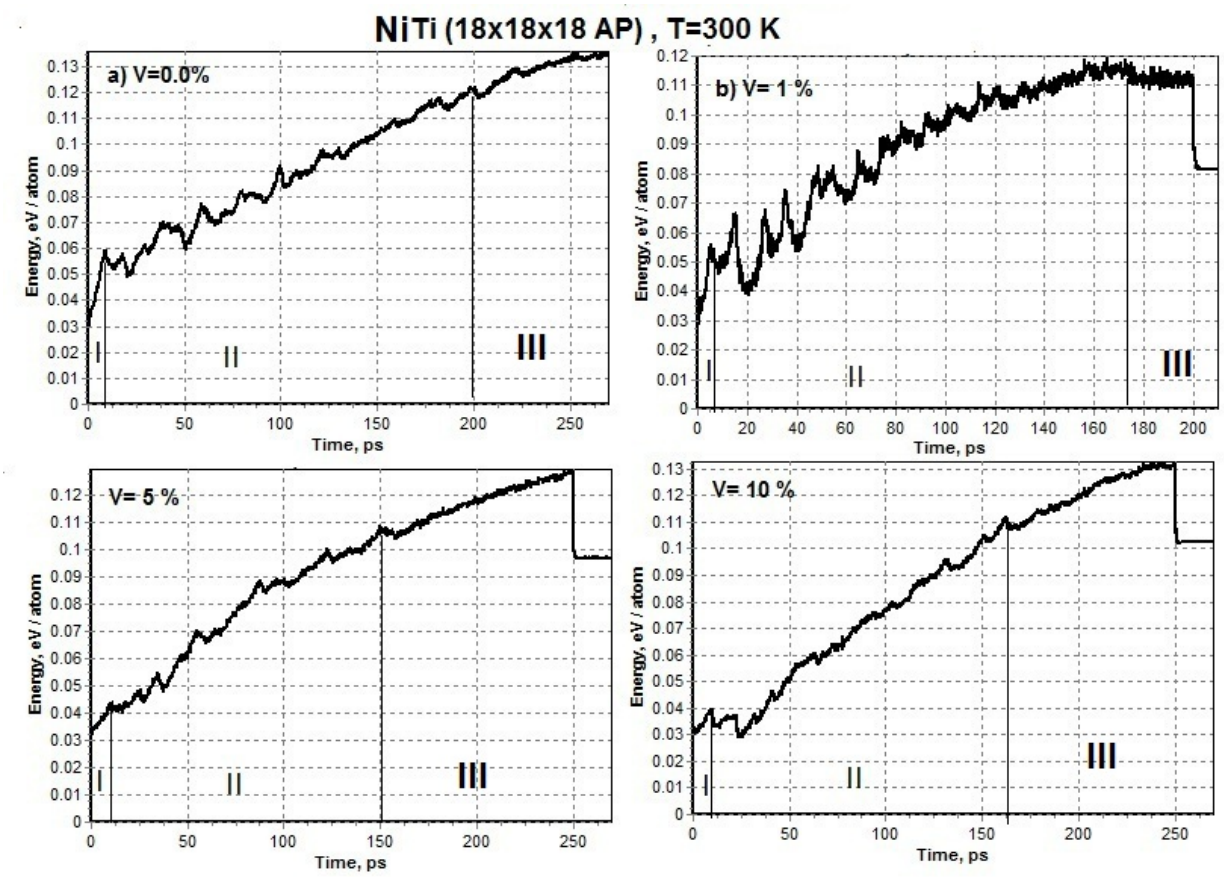

Fig. 4. The dependence of the stored energy of deformation at 300 K for NiTi 18 x 18 x 18 AP using Cleri-Rosato potential [11], a) without vacancies, b) V = 1%, c) V = 5% and d) V = 10%

Tensile deformation. The mechanical properties at different vacancy rates with MD simulations are studied (Table 3), the uniaxial tension of the Ni and Ti nanowires and Nitinol alloys are studied with different vacancy rates at 300 K and 1000K. Figure 5 gives the stress–strain relationships of the (12 x 12 x 12 AP FCC) Ni nanowires subjected to uniaxial tension at different vacancies rate at temperatures 300 K and 1000K. The effect of vacancy rates on the stress strain curve of the (12 x 12 x 12 AP) HCP Ti nanowires was shown in Fig. 6 at temperatures 300 K and 1000K. Figure 7 gives the stress–strain relation of the (18 x 18 x 18 AP) Nitinol alloys at various vacancy rates at 300 K and 1000K.

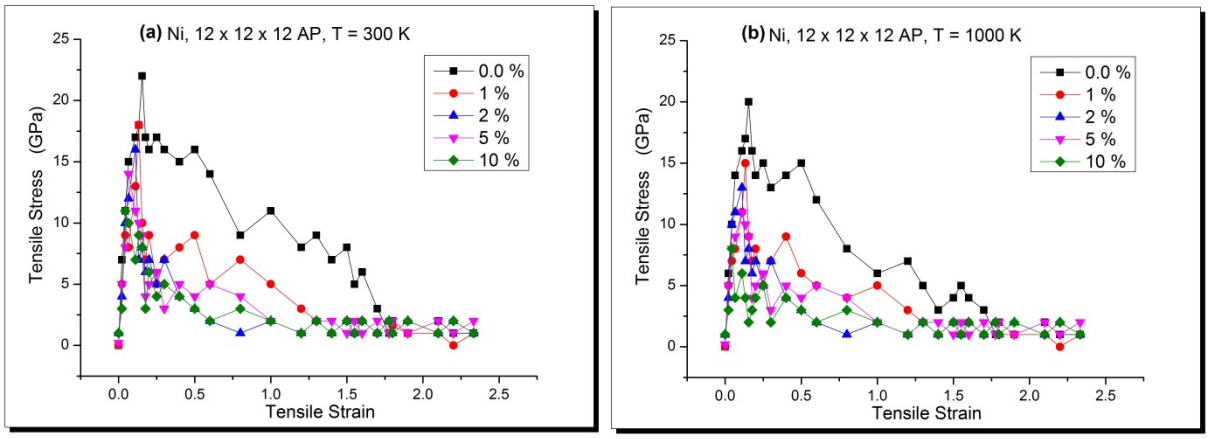

Fig. 5. Tensile stress vs. tensile strain for FCC Ni 12 x 12 x 12 AP nanowires at various vacancy rates at (a) 300 K, (b) 1000 K

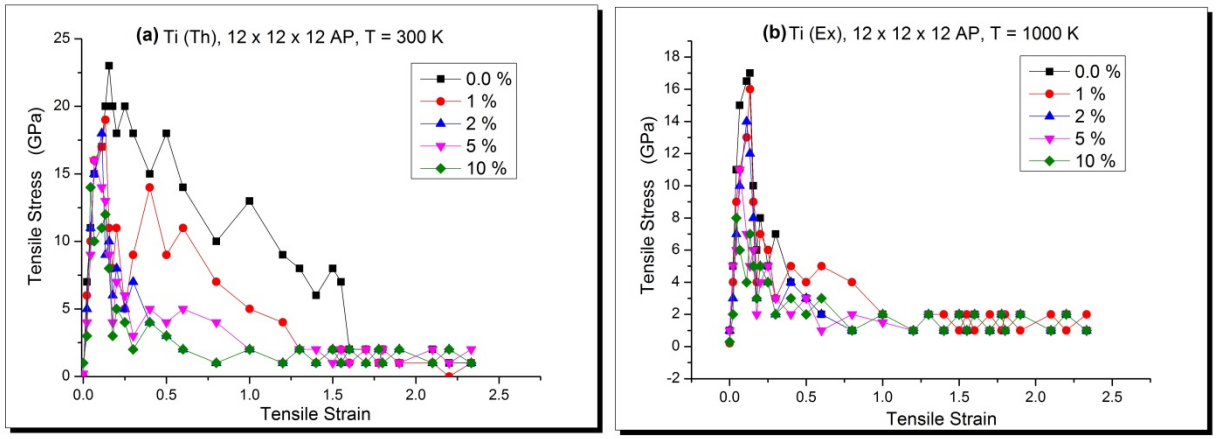

Fig. 6. Tensile stress vs. tensile strain for HCP Ti nanowires at various vacancy rates at (a) 300 K, (b) 1000 K

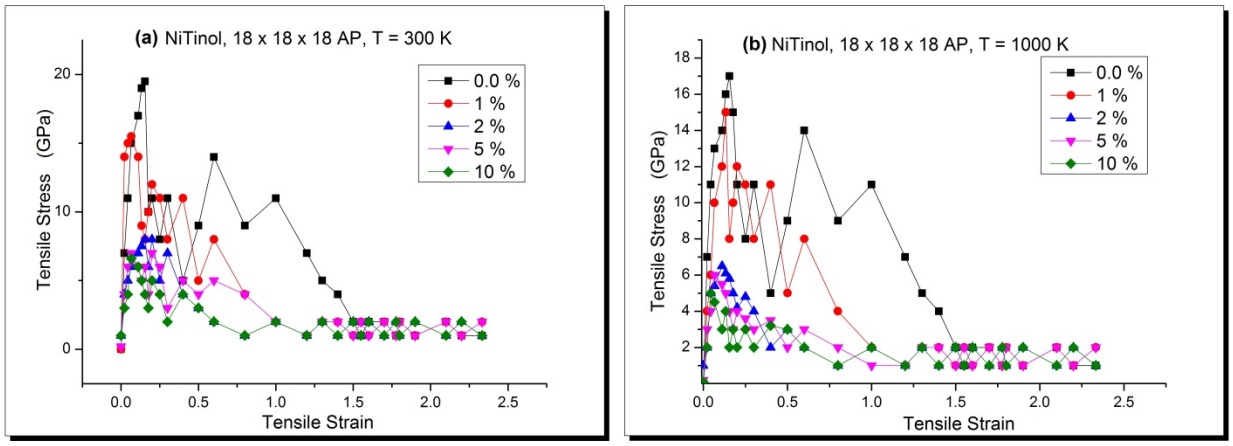

Fig. 7. Tensile stress vs. tensile strain for NiTi alloys at various vacancy rates at (a) 300 K, (b) 1000 K

With the increasing initial strain, stress increases linearly at various vacancies. This process corresponds to the elastic deformation of the nanowires. With the increasing strain, stress decrease as shown in the stress–strain response of the nanowires, indicating the beginning of the plastic deformation of the nanowire. The stress–strain curves are smooth at

no vacancies, some "minipeaks" exhibit with increasing vacancy rates. The results demonstrate that the tensile strength decreases with increasing vacancy rates.

Deformation of the nanowires is in a fast stage of the atomic damage process. It was observed that the yield stress decreases as the vacancy number increases (Fig. 8). When the plastic deformation of the nanowire begins, the drop of the first yield stress also decreases. Figure 8 shows the simulated ultimate strength of Ni and Ti (for both experimental and theoretical parameters) nanowire and Nitinol alloy as a function of vacancy rates. As expected, the nanowire strength decreases with increase the vacancy number.

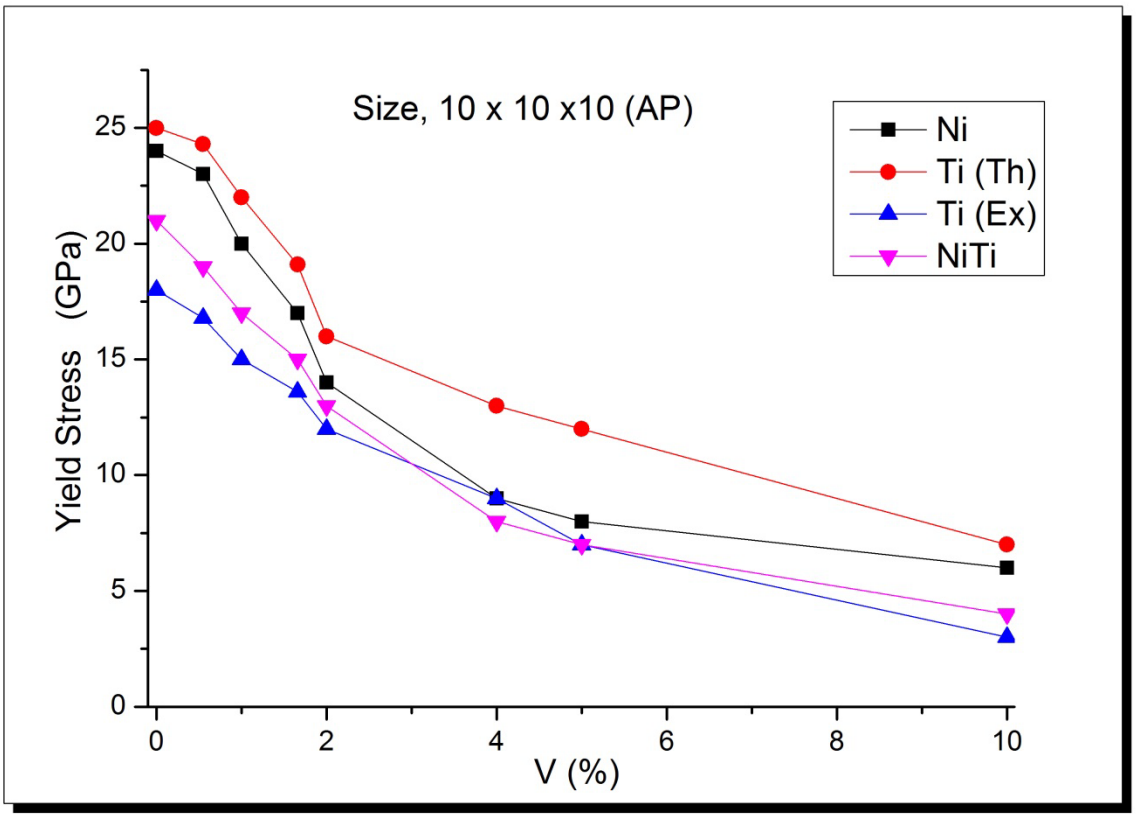

Fig. 8. Relationship between yield strength for 10 x 10 x 10 AP Ni and Ti (theoretical and experimental values) nanowires and Nitinol alloys with various vacancy rates at T=300 K

Breaking time and position. The results showed that the breaking time depended on the vacancy rates as in Fig. 9. The most probable breaking position was located at the center of the nanowires. Figure 9 presents the calculated breaking time for 10 x 10 x 10 AP Ni and Ti (theoretical and experimental values) nanowire and Nitinol alloys as a function of vacancy rates.

If the breaking position and breaking time are predictable, the nanowire can be strengthened near the breaking position and time to avoid failure. Although the single breaking case is not predictable, many breaking cases show a statistic feature. Figures 10 and 11 presents the representative snapshots of 12 x 12 x 12 AP Ti nanowire and for 18 x 18 x 18 Ap Nitinol alloys with different vacancies at the breaking moment at 300 K, respectively. In most cases, the final breaking position occurs at the central part of this Ti nanowire but for NiTinol the position gradually shifts to the ends.

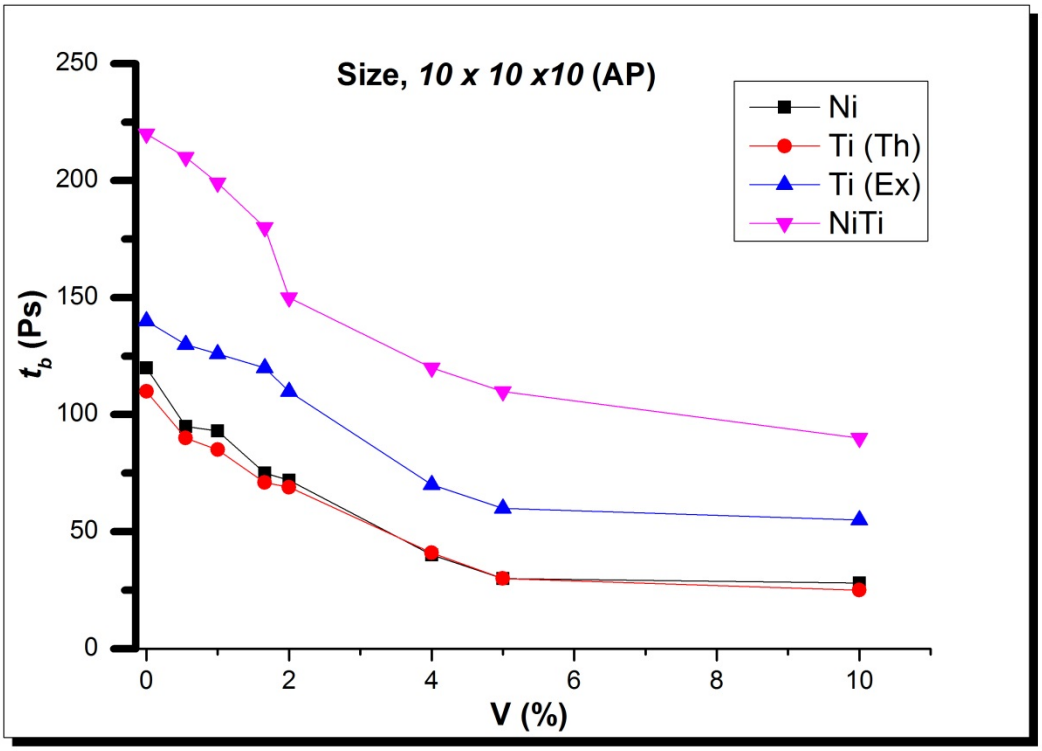

Fig. 9. Relationship between breaking time for 10 x 10 x 10 AP Ni and Ti (theoretical and experimental values) nanowire and Nitinol alloys with various vacancies at T=300 K

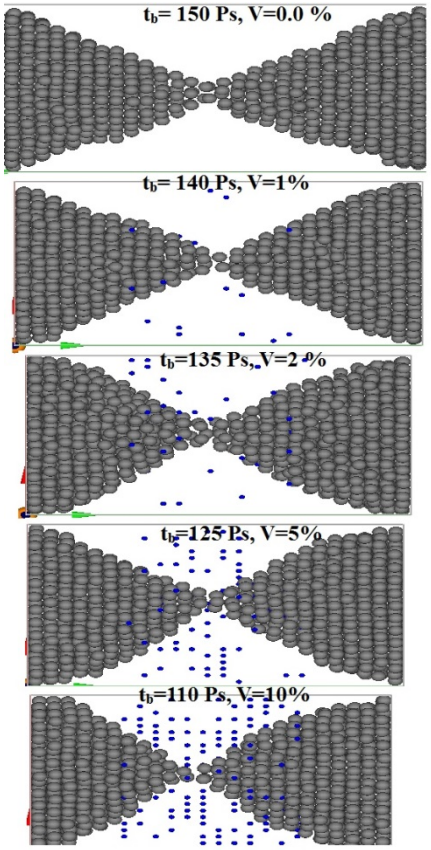

Fig. 10. Snapshots of 12 x 12 x 12 (AP) Ti alloy with different vacancies and the breaking moment at 300K

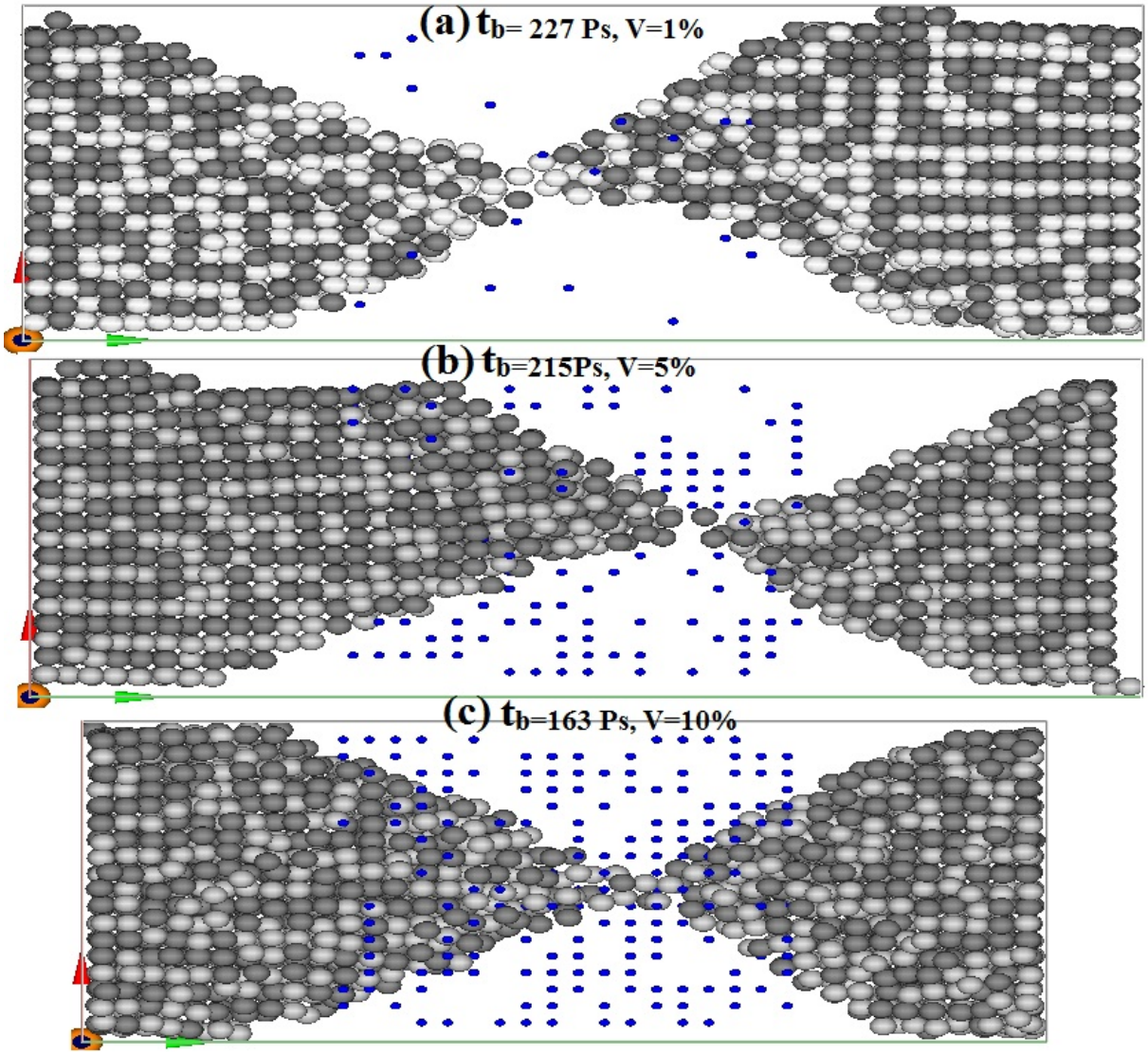

Fig. 11. Snapshots of 18 x 18 x 18 (AP) NiTinol alloy with different vacancies and the breaking moment at 300K

4. Conclusion

In this work, MD simulations are performed for Ni and Ti nanowire and Nitinol alloy subject to uniaxial tensile strain loading. A many-body interatomic potential within the second-moment approximation of the tight-binding model (the Cleri and Rosato potentials) was employed to carry out three dimensional molecular dynamics simulations. MD simulation results at 300K and 1000K temperature were presented. The stress–strain curves for nanowires were simulated. The breaking and yield stress of nanowires are dependent on the size, temperature and vacancy rates.

The tensile stress decreases with increasing vacancy fraction of the material and the maximum stress founded at zero vacancies. The studied materials shows very high ultimate tensile stress and elongation rate. Increasing vacancy fraction was also affect the yield stress to decrease. It was observed that the Ni and Ti nanowires and Nitinol alloys has a higher fatigue limit when the vacancy fraction is lower, and when the value of applied stress is less-than-critical.

The necking, plastic deformation and breaking of nanowires are demonstrated. The effect of temperature was successfully studied; the elastic modulus and the stress were

linearly decreased. The simulation results would be helpful to avoid the materials failure by predicting the breaking position. This study of mechanical properties of metal nanowires will be helpful to the design, manufacture and manipulation of nano-devices.

Acknowledgements. *No external funding was received for this study.*

References

[1] Feng G, Nix WD, Yoon Y, Lee CJ. A study of the mechanical properties of nanowires using nanoindentation. *J. Appl. Phys*. 2006;99(1): 074304.
[2] Wang ZL, Dai ZR, Gao RP, Bai ZG, Gole JL. Side-by-side silicon carbide–silica biaxial nanowires: Synthesis, structure, and mechanical properties. *Appl. Phys. Lett.* 2000;77(21): 3349.
[3] Starostenkov MD, Aish MM. Effect of Length and Cross-Sectional Area on Ni_3Fe Alloy Plasticity. *Advanced Materials Research*. 2014;1013(1): 242-248.
[4] Aish MM, Starostenkov MD. Mechanical properties of metallic nanowires using tight-binding model. *AIP Conf. Proc*. 2016;1698: 040006.
[5] Starostenkov MD, Aish MM. Molecular dynamic study for ultrathin Nickel nanowires at the same temperature. *Materials Physics and Mechanics*. 2014;21(1): 1-7.
[6] Starostenkov MD, Aish MM, Sitnikov AA, Kotrechko SA. Deformation of different nickel nanowires at 300 K. *Letters on Materials.* 2013;3(3): 180.
[7] Starostenkov MD, Aish MM. Feature deformation and breaking of Ni nanowire. *Letters on Materials.* 2014;4(2): 89.
[8] Starostenkov MD, Aish MM. Effect of volume on the mechanical properties of nickel nanowire. *Materials Physics and Mechanics.* 2013;18(1): 53-62.
[9] Starostenkov MD, Aish MM. Deformation and Fracture of Metallic Nanowires Solid State. *Phenomena*. 2017;258(1): 277-280.
[10] Aish MM, Shatnawi MTM, Starostenkov MD. Characterization of strain-induced structural transformations in CdSe nanowires using molecular dynamics simulation. *Materials Physics and Mechanics.* 2015;24(4): 403-409.
[11] Cleri F, Rosato V. Tight-binding potentials for transition metals and alloys. *Phys. Rev. B.* 1993;48(1): 22-33.
[12] Aish MM, Starostenkov MD. Features of structural transformations of HCP metallic Ti nanowires using Cleri-Rosato potential at low temperature. *Letters on Materials*. 2016;6(4): 317.
[13] Rexer EF, Jellinek J, Krissinel EB, Parks EK. Theoretical and experimental studies of the structures of 12-, 13-, and 14-atom bimetallic nickel/aluminum clusters. *J. Chem. Phys.* 2002;117(1): 82.
[14] Darby S, Mortimer-Jones TV, Johnston RL, Roberts C. Theoretical study of Cu–Au nanoalloy clusters using a genetic algorithm. *J. Chem. Phys.* 2002;116: 1536.
[15] Michaelian K, Beltran MR, Garzon IL. Disordered global-minima structures for Zn and Cd nanoclusters. *Phys. Rev. B.* 2002;65: 041403(R).
[16] Gades H, Urbassek HM. Preferential sputtering of alloys: a molecular-dynamics study. *Nucl. Instr. Meth. B.* 1995;102(1-4): 261.
[17] Hobbs L. Point defect stabilization in ionic crystals at high defect concentrations. *Journal de Physique Colloques.* 1976;37(C7): C7-3 - C7-26.
[18] Mazzone G, Rosato V, Pintore M. Molecular-dynamics calculations of thermodynamic properties of metastable alloys. *Phys. Rev. B.* 1997;55: 837.
[19] Levanov K, Stepanyuk VS, Hergert W, Trushin S, Kokko K. Molecular dynamics simulation of Co thin films growth on Cu(001). *Surface Science.* 1998;400(1): 54-62.
[20] Garrison BJ, Winograd N, Deaven DM, Reimann CT, Lo DY, Tombrello TA, Harrison DE Jr, Shapiro MH. Many-body embedded-atom potential for describing the energy and angular distributions of Rh atoms desorbed from ion-bombarded Rh{111}. *Phys. Rev. B.* 1988;37(13): 7197-7204.
[21] Rafi-Tabar H, Sutton AP. Long-range Finnis-Sinclair potentials for f.c.c. metallic alloys. *Phil. Mag. Lett.* 1991;63: 217-224.
[22] Daw MS, Foiles SM, Baskes M. The embedded-atom method: a review of theory and applications. *Materials Science Reports.* 1993:9(7): 251-310.